Supporting Appendix

Section 1. Experimental and synthetic details.

Synthesis of 4,4'-bis(11-mercaptoundecanoxy)azobenzene [ADT]

11-Thioacetoxyundecanol

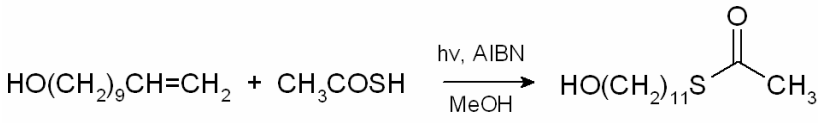

A mixture of undec-10-enol (12.00 g), thioacetic acid (20 mL) and AIBN (80 mg) was dissolved in methanol (50 mL) and irradiated with a 450 W Hg arc lamp in a quartz reactor under nitrogen atmosphere for 16 h. The reaction mixture was then concentrated *in vacuo*. The residue was purified by column chromatography (chloroform-petroleum ether 3:1). Yield: 5.39 g (31%). ^{1}H NMR: (DMSO-d_6, 300 MHz) δ 4.29 (br, 1H), 3.36 (t, 2H, J = 6.3 Hz), 2.81 (t, 2H, J = 7.2 Hz), 2.30 (s, 3H), 1.51-1.23 (m, 18H).

11-Thioacetoxy-1-bromoundecane

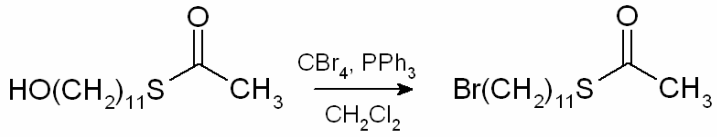

To a cooled solution of 11-thioacetoxyundecanol (2.0 g) and triphenylphosphine (5.3 g) in anhydrous (distilled over P_4O_{10}) dichloromethane (30 mL) was added a solution of tetrabromomethane (4.2 g) in anhydrous dichloromethane (15 mL). Stirring was continued for 24 h at room temperature. The solvent was evaporated *in vacuo* and the residue extracted (five times) with petroleum ether. The crude product was purified by column chromatography (1:50 ethyl acetate-hexanes). Yield: 1.81 g (72%). ^{1}H NMR: (acetone-d_6, 300 MHz) δ 3.51 (t, 2 H, J = 6.6 Hz), 2.87 (t, 2 H, J = 7.2 Hz), 2.31 (s, 3 H), 1.87 (t, 2H, J = 7.2 Hz), 1.65-1.15 (m, 16H).

4,4'-Dihydroxyazobenzene

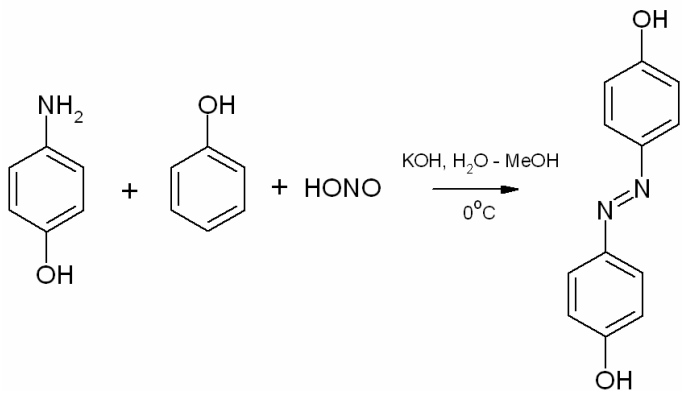

4-Hydroxyaniline was dissolved in 170 mL of 1 M HCl and cooled to 0°C. A solution of KNO_2 (11.27 g in 34 mL H_2O) was added dropwise under constant stirring. The mixture was diluted by adding 340 mL pre-cooled methanol. In a separate batch, phenol (9.24 g) and KOH (10.42 g) were dissolved in 48 mL methanol and cooled to 0°C. This phenolate solution was added dropwise under constant stirring. The resulting red solution was stirred for additional 24 h. 1 M HCl was added to precipitate the crude product, which was collected by filtration. The crude product was then recrystallized from glacial acetic acid. Yield: 5.515 g (53%). ^{1}H NMR: (DMSO-d_6, 300 MHz) δ 10.10 (s, 2H), 7.75 (d, 4H, J = 8.4 Hz), 6.90 (d, 4H, J = 8.4 Hz).

4,4'-Bis(11-thioacetoxyundecanoxy)azobenzene

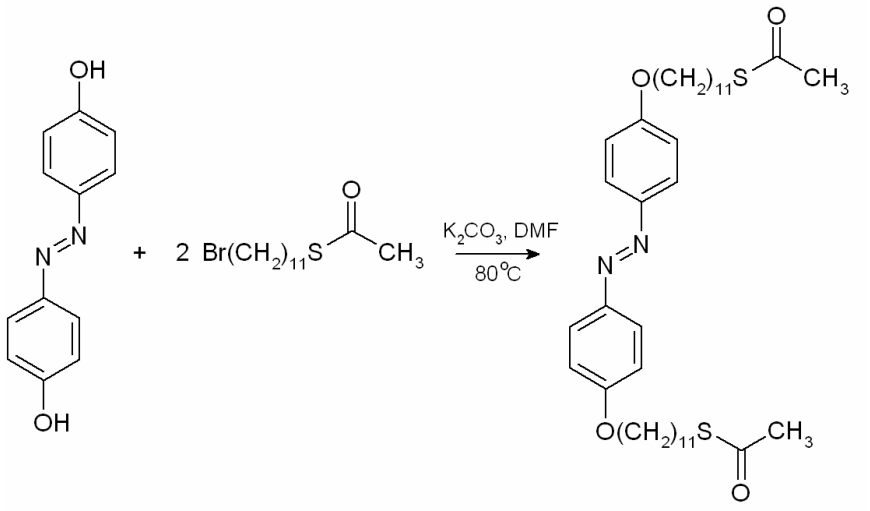

On the basis of (1). 4,4'-dihydroxyazobenzene (150 mg; 1 eq) and 11-thioacetoxy-1-bromoundecane (465 mg; 2.14 eq) were dissolved in freshly distilled DMF (11 mL). K_2CO_3 (386 mg) and KI (catalytic amount) were added and the mixture was stirred under nitrogen atmosphere at 80°C for 4 h. Solvent was removed *in vacuo* and the residue was dissolved in dichloromethane and washed (three times) with water. The solution was dried ($MgSO_4$) and the solvent was evaporated. The crude product was purified by column chromatography (1:10 ethyl acetate-hexanes). Yield: 390 mg (83%). ^{1}H NMR: ($CDCl_3$, 300 MHz) δ 7.81 (d, 4H, *J* = 8.7 Hz), 6.99 (d, 4H, *J* = 8.7 Hz), 4.04 (t, 4H, *J* = 6.6 Hz), 2.87 (t, 4H, *J* = 7.2 Hz), 2.33 (s, 6H), 1.95-1.05 (m, 36H).

4,4'-Bis(11-mercaptoundecanoxy)azobenzene

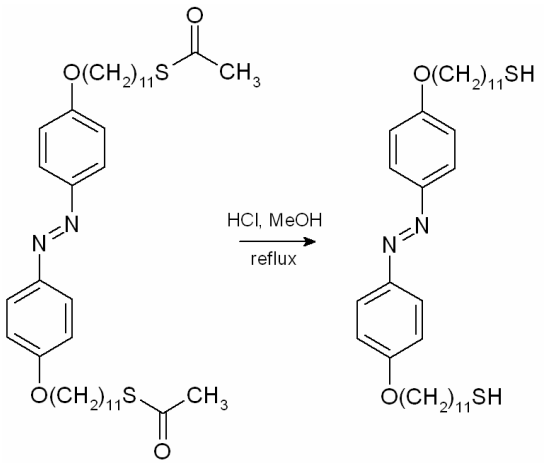

4,4'-Bis(11-thioacetoxyundecanoxy)azobenzene (400 mg) was dissolved in chloroform-methanol mixture (5 mL : 15 mL) and 2.5 M HCl solution in methanol (20 mL) was added. The mixture was refluxed in nitrogen atmosphere for 4h. After that time, the reaction mixture was concentrated *in vacuo* and the crude product was purified by column chromatography (1:5 dichloromethane-hexanes). Yield: 311 mg (89%). ^{1}H NMR: ($CDCl_3$, 300 MHz) δ 7.94 (d, 4H, J = 9.0 Hz), 7.00 (d, 4H, *J* = 9.0 Hz), 4.06 (t, 4H, *J* = 6.3 Hz), 2.54 (q, 4H, *J* = 7.4 Hz), 2.05-0.90 (m, 36H). ESI-MS: 587.4 ($M+H^+$).

(iii) Synthesis of 4-(undec-10-enoxy)-4'-(11-mercaptoundecanoxy)azobenzene [BAD]

4-Hydroxy-4'-(11-thioacetoxyundecanoxy)azobenzene

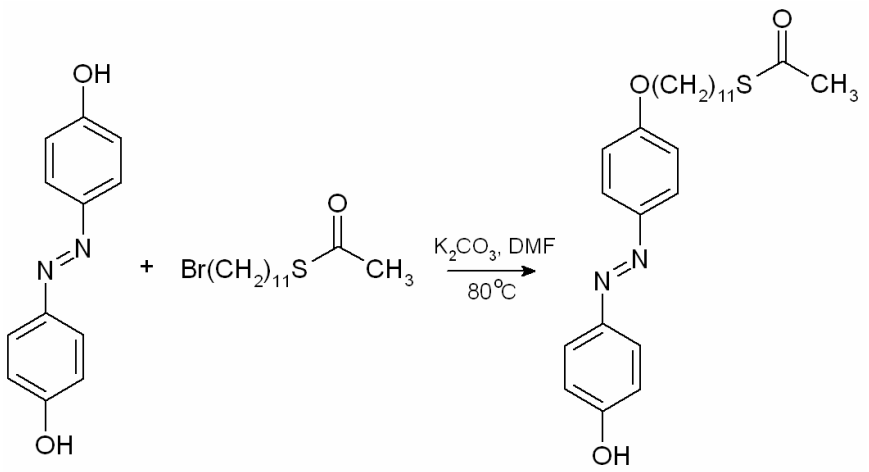

11-Thioacetoxy-1-bromoundecane (868 mg; 1.00 eq) dissolved in freshly distilled DMF (20 mL) was added dropwise to a mixture of 4,4'-dihydroxyazobenzene (1.09 g; 1.82 eq), K_2CO_3 (1,41 g; 6.64 eq) and KI (catalytic amount) in distilled DMF (20 mL). Stirring was continued overnight under nitrogen atmosphere at T = 80°C. Solvent was removed *in vacuo* and the residue was dissolved in dichloromethane and washed (three times) with water. The solution was dried ($MgSO_4$) and the solvent was evaporated. The crude product was purified by column chromatography (1:4 ethyl acetate-hexanes). Yield: 942 mg (76%). ^{1}H NMR: ($CDCl_3$, 300 MHz) δ 7.87 (t, 4H, J = 8.4 Hz), 6.98 (q, 4H, J = 4.2 Hz, 9.0 Hz), 5.5 (br, 1H), 4.04 (t, 2H, J = 6.6 Hz), 2.88 (t, 2H, J = 6.9 Hz), 2.34 (s, 3H), 1.82 (m, 2H), 1.85-1.05 (m, 16H).

4-(Undec-10-enoxy)-4'-(11-thioacetoxyundecanoxy)azobenzene

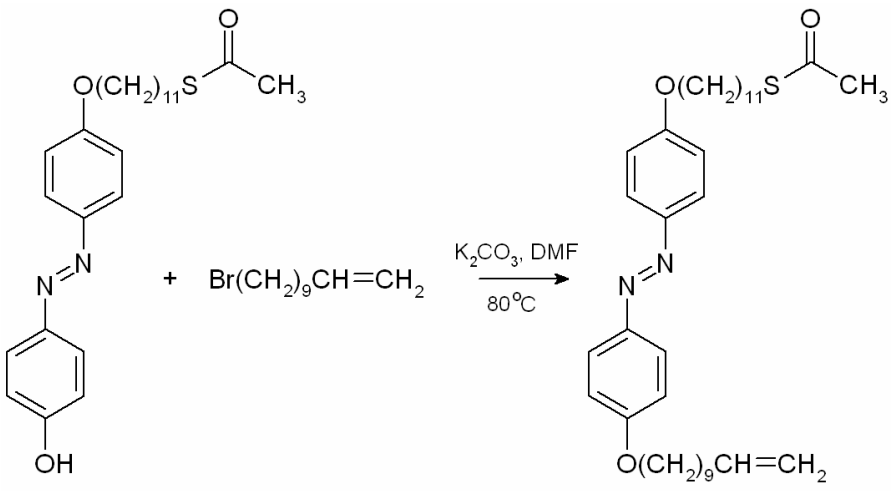

4-Hydroxy-4'-(11-thioacetoxyundecanoxy)azobenzene (204 mg; 1.00 eq) and 11-thioacetoxy-1-bromoundecane (216 mg; 2.00 eq) were dissolved in freshly distilled DMF (15 mL). K_2CO_3 (255 mg; 4.00 eq) and KI (catalytic amount) were added and the mixture was stirred under nitrogen atmosphere at 80°C for 4 h. Solvent was removed *in vacuo* and the residue was dissolved in dichloromethane and washed (three times) with water. The solution was dried ($MgSO_4$) and the solvent was evaporated. The crude product was purified by column chromatography (1:20 ethyl acetate-hexanes). Yield: 186 mg (68%). ^{1}H NMR: ($CDCl_3$, 300 MHz) δ 7.87 (d, 4H, J = 8.7 Hz), 6.99 (d, 4H, J = 8.7 Hz), 5.78 (tt, 1H), 4.96 (dd, 2H), 4.04 (t, 4H, J = 6.9 Hz), 2.87 (t, 2H, J = 7.5 Hz), 2.33 (s, 3H), 2.00 (dt, 2H), 1.9-1.0 (m, 32H).

4-(Undec-10-enoxy)-4'-(11-mercaptoundecanoxy)azobenzene

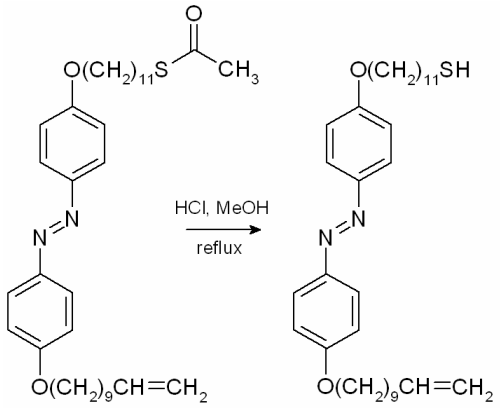

4-(Undec-10-enoxy)-4'-(11-thioacetoxyundecanoxy)azobenzene (185 mg) was dissolved in 20 mL of 0.1 M HCl solution in methanol. The mixture was refluxed under nitrogen atmosphere for 4 h. After that time, the reaction mixture was concentrated *in vacuo* and the crude product was purified by column chromatography (1:5 ethyl acetate-hexanes). Yield: 144 mg (84%). ^{1}H NMR: ($CDCl_3$, 300 MHz) δ 7.89 (d, 4H, J = 8.7 Hz), 7.00 (d, 4H, J = 8.7 Hz), 5.77 (tt, 1H), 4.94 (dd, 2H), 4.04 (t, 4H, J = 6.9 Hz), 2.55 (q, 4H, J = 7.3 Hz), 1.98 (dt, 2H), 1.9-1.0 (m, 32H). ESI-MS: 553.8 ($M+H^+$).

Section 2. Detailed discussion of interparticle interactions.

The interaction energy between two *cis*-ADT-coated NPs in a toluene/methanol environment can be estimated as the adhesion energy gained by bringing the NPs into close contact. This energy may be expressed as $E_{\mathrm{ad}} = A_{\mathrm{eff}}(\sigma_{11} - 2\sigma_{12})$, where A_{eff} is the effective area of contact between the two spheres, σ_{11} is the surface energy of the NP-NP interface (here, due primarily to dipole-dipole interactions), and σ_{12} is the surface energy of the NP-solvent interface. In other words, upon contact between NPs, one NP-NP interface is created at the expense of two NP-solvent interfaces.

The effective area of contact, A_{eff}, between two spheres of radius R interacting via short-range forces (here, dipole-dipole and solvophobic) with a characteristic molecular scale a (here, a ~ 5Å, corresponding to closest dipole-dipole spacing, cf. Fig 7) can be approximated as $A_{\mathrm{eff}} \approx 2\pi Ra$ (2). To estimate σ_{11}, we consider each NP to be uniformly covered with a given number, N_{azo}, of *cis*-azobenzene dipoles. Assuming the spatial distributions of ligands are random and uncorrelated between the NPs, the number of dipole-dipole pairs per unit area at contact may be estimated as $\rho_{dd} = N_{azo}/4\pi R^2$. Thus, the energy per unit area at contact is estimated to be $\sigma_{11} = N_{azo}E_{dd}/4\pi R^2$, where E_{dd} is the energy of a single dipole-dipole pair.

The pairwise dipole-dipole energy is given by the following expression, in which μ is the dipole moment (here, μ = 4.4 D), ε_0 is the dielectric permittivity of vacuum, ε is the dielectric constant of the medium (e.g., $\varepsilon_{\mathrm{toluene}} = 2.379$), k is Boltzmann's constant, T is temperature, and r is the distance between dipoles (here, $r = a$ ~ 5Å).

$$E_{dd}(r,\theta_1,\theta_2,\phi) = -(\mu^2/4\pi\varepsilon_0\varepsilon r^3)(2\cos\theta_1\cos\theta_2 - \sin\theta_1\sin\theta_2\cos\phi)$$

Here, the relative orientation of the two dipoles is defined by the angles θ_1, θ_2, and ϕ as illustrated in Fig. 5 below.

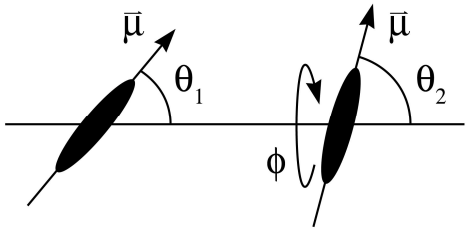

Figure 5. Schematic illustration of two dipoles and their angles of orientation, θ_1, θ_2, and ϕ.

Because the characteristic magnitude of this interaction is only slightly greater than kT (i.e., $\mu^2/4\pi\varepsilon_0\varepsilon a^3$ ~ 0.9 kcal/mol and kT ~ 0.6 kcal/mol), it is appropriate to consider the angle-averaged dipole-dipole potential for freely rotating dipoles (2):

$$E_{dd}(r) = -kT \ln\left\langle \exp[-E_{dd}(r,\theta_1,\theta_2,\phi)/kT]\right\rangle .$$

Here, the angled brackets denote an average over all possible orientations.

$$\left\langle \exp[-E_{dd}(r,\theta_1,\theta_2,\phi)/kT]\right\rangle = \frac{1}{8\pi}\int_0^{2\pi} d\phi \int_0^{\pi} \sin\theta_1 d\theta_1 \int_0^{\pi} \exp[-E_{dd}(r,\theta_1,\theta_2,\phi)/kT]\sin\theta_2 d\theta_2$$

The above relation may be simplified for dipole-dipole energies significantly greater than or less than the thermal energy.

$$E_{dd}(r) = \frac{-\mu^2}{2\pi\varepsilon_0\varepsilon r^3} \qquad \text{for } \frac{\mu^2}{4\pi\varepsilon_0\varepsilon r^3} >> kT \text{ (“Frozen” Dipole Interaction)}$$

$$E_{dd}(r) = \frac{-1}{3kT}\left(\frac{\mu^2}{4\pi\varepsilon_0\varepsilon r^3}\right)^2 \qquad \text{for } \frac{\mu^2}{4\pi\varepsilon_0\varepsilon r^3} << kT \text{ (Keesom Interaction)}$$

Fig. 6 compares these approximate forms with the numerically computed potentials for the parameters of the present system.

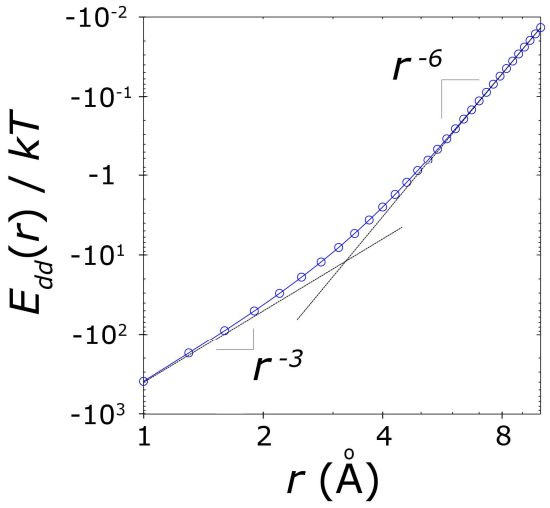

Figure 6. Angle averaged dipole-dipole energy relative to kT as a function of the dipole separation distance r. Here, μ = 4.4 D, $\varepsilon_{\text{toluene}} = 2.379$, and T = 293 K. The black lines correspond to the approximate interaction potentials: “frozen” dipole interaction (r^{-3} dependence) and Keesom interaction (r^{-6} dependence).

From the plot, we find that the approximate Keesom interaction is accurate to within 10% at the minimum dipole-dipole separation distance, a ~ 5 Å; therefore, we use this relation for all subsequent calculations – specifically, $E_{dd}(a) \approx 3.5\times10^{-21}$ J .

The surface energy of the NP-solvent interface, σ_{12}, is estimated in a more heuristic manner from interfacial energies of similar interfaces previously reported in the literature. Importantly, we note that while the NP surface may be covered by a significant number of *cis*-ADT molecules, it is still effectively hydrophobic due to the long *n*-alkane chains of DDA molecules as well as the "free" *n*-alkane chains of *cis*-ADT ligands – this effective hydrophobicity is evidenced by experimental observation that the NPs are less stable when the content of (polar) methanol, *x*, increases and that they precipitate above $x \sim 30\%$. It is therefore reasonable to assume that surface energy of the NP-solvent interface is largely due to *n*-alkane/solvent interactions. In this case, it can be approximated by a linear average of the *n*-alkane-toluene and the *n*-alkane-methanol surface energies: $\sigma_{12} = (1-x)\sigma_{\text{alk-tol}} + x\sigma_{\text{alk-meth}}$, where *x* is the volume fraction of methanol in the solvent, $\sigma_{\text{alk-tol}} \sim 0.1$ mJ/m^2 (estimated by the relation $\sigma_{AB} = \sigma_A + \sigma_B - 2\sqrt{\sigma_A \sigma_B}$), and $\sigma_{\text{alk-meth}} \sim 1.3$ mJ/m^2 (average $\sigma_{\text{alk-meth}}$ for *n*-alkanes and methanol for $n = 6$-12) (3). Furthermore, since $\sigma_{\text{alk-tol}} << \sigma_{\text{alk-meth}}$, it is neglected in all subsequent calculations.

In sum, the adhesion energy between two NPs is given as follows.

$$E_{\text{ad}} = -A_{\text{eff}} \left(\frac{E_{dd} N_{\text{azo}}}{4\pi R^2} + 2(1.3 \text{ mJ m}^{-2})x \right)$$

Substituting numerical values for the various parameters, this expression becomes:

$$E_{\text{ad}} = -\left[(0.045 \text{ kcal/mol}) N_{\text{azo}} + (3.3 \text{ kcal/mol}) x \right]$$

Therefore, for pure toluene ($x = 0$), the adhesion energy is comparable to the thermal energy of an NP ($3/2kT$) when $N_{\text{azo}} \sim 19$, which is close to our experimental estimate of ~16 ADT molecules per NP necessary for forming aggregates (cf. Fig. 1A). Also, considering the case in which there is no ADT in solution, the above relation predicts that the adhesion energy is comparable to the thermal energy for a methanol fraction of ~0.3, which agrees with the experimental observation that NPs precipitate for methanol fractions above 0.28 (irrespective of ADT concentration). Note, however, that this relation is qualitatively inaccurate for predicting the slope of the boundary between the free NP phase and the IC phase.

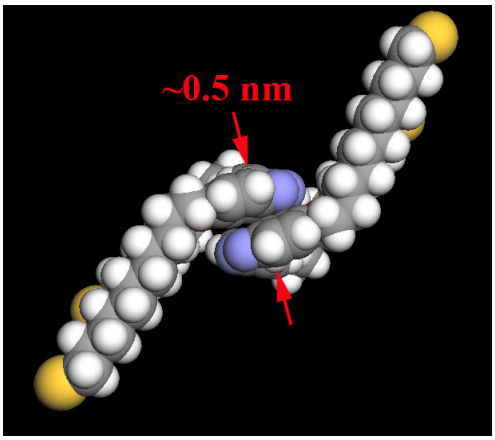

Figure 7. Two *cis*-ADT ligands with their azobenzene units stacked on "on-top" of one another. The energy of the structure was minimized using CHARMM force-field and with the conformations of the side-chains constrained.

Section 3. Determination of the binding energy of DDA capping agents from digestive ripening experiments.

Since the binding energy of amine-terminated capping agents (e.g., DDA) on AuNPs relative to that of thiol ligands has not been previously reported, we used a slightly modified version of the model of Heath and Gelbart (4) to determine binding energies from the thermodynamics of a digestive ripening process.

It is well known that heating of polydisperse AuNPs in the presence of a stabilizing ligand, such as dodecanethiol or dodecylamine, can lead to monodisperse nanoparticles via a process called digestive ripening (5). Here, the distribution of particle sizes is determined entirely by thermodynamic considerations, and the same size distribution is achieved regardless of the shapes and sizes of the initial NPs (4). The final size distribution can be understood qualitatively as a balance between the surface energy of the gold particles (favors large particles to minimize total surface area of the ensemble) and the binding energy of the ligands (favors smaller particles onto which more ligands can be adsorbed). For example, digestive ripening experiments – reported by others (5) and also confirmed by our group – have shown that dodecanethiol and dodecylamine stabilized NPs have average diameters equal to 4.7 nm and 8.6 nm, respectively, implying that the binding energy of the thiol is greater than that of the amine. To obtain a quantitative estimate on the difference between the binding energies of dodecanethiol and dodecylamine, we used a statistical thermodynamic theory that describes the surfactant-mediated size control of Au nanoparticles. As this theory has been described in detail elsewhere (4), we outline only its basic concepts and extensions relevant to the present study.

Consider an ideal solution of N_g gold atoms organized into spherical particles, N_s surfactant molecules (i.e., dodecanethiol or dodecylamine), and N_o solvent molecules. A given particle contains n gold atoms and is stabilized by n_s surfactant molecules. The free energy, F, of this system is expressed as

$$F = \sum_n \left(N_n \mu_n - k_B T N_n\right) + N_{1,s}\mu_{1,s}$$

Where N_n is the number of particles containing n gold atoms, μ_n is the chemical potential of such a particle (cf. below), $N_{1,s}$ is the number of monomeric (free) surfactant molecules, $\mu_{1,s}$ is their chemical potential, k_B is Boltzmann's constant, and T is temperature. Furthermore, since we assume that our solution is ideal, we have the following relations.

$$\mu_n = \mu_n^o + k_B T \ln(N_n / N_t) \text{ and } \mu_{1,s} = \mu_{1,s}^o + k_B T \ln(N_{1,s} / N_t)$$

Here, μ_n^o and $\mu_{1,s}^o$ are standard chemical potentials, and N_t is the total number of molecules in solution ($N_t = N_g + N_s + N_o$).

The system is subject to two constraints arising from the conservation of the total number of gold atoms and surfactant molecules, respectively.

$$\sum_{n=1} nN_n = N_g \text{ and } \sum_{n=1} n_s(n)N_n + N_{1,s} = N_s$$

Therefore, the task is now to find the distribution of particle sizes that minimizes the free energy subject to the above constraints.

$$\frac{\partial E}{\partial N_n} = 0 = \mu_n^o + k_B T \ln(N_n / N_t) - \lambda n - \lambda^* n_s$$

Where λ and λ^* are Lagrangian multipliers associated with the two constraints above (physically, they are exactly the chemical potentials of gold and surfactant, respectively). From the relation above we can find the mole fraction, X_n, of gold atoms within particles of size n and the distribution of particle sizes.

$$X_n / n = N_n / N_t = \exp\left[(-\mu_n^o + \lambda n + \lambda^* n_s) / k_B T\right]$$

Likewise, for the monomeric surfactant molecules we obtain the following.

$$X_{1,s} = N_{1,s} / N_t = \exp\left[(-\mu_{1,s}^o + \lambda^*) / k_B T\right]$$

Furthermore, these expressions can be simplified by way of the following arguments. The chemical potential of an n-sized particle is approximated as

$$\mu_n^o = (n - n_{out})\mu_{bulk,g}^o + n_{out}\mu_{out,g}^o + n_s \mu_{out,s}^o$$

Where n_{out} are the number of gold atoms at the particle surface, and $\mu_{bulk,g}^o$, $\mu_{out,g}^o$, and $\mu_{out,g}^o$ are the chemical potentials of bulk gold, surface gold, and surface-bound surfactant molecules, respectively. Re-defining chemical potentials relative to that of bulk gold ($\mu_{bulk,g}^o$) and that of free surfactant ($\mu_{1,s}^o$), $\alpha = \lambda - \mu_{bulk,g}^o$ and $\alpha^* = \lambda - \mu_{1,s}^o$, we can now express X_n and $X_{1,s}$ as follows.

$$X_n / n = N_n / N_t = \exp\left[(-\sigma_n + \alpha n + \alpha^* n_s) / k_B T\right]$$

$$X_{1,s} = N_{1,s} / N_t = \exp\left[\alpha^* / k_B T\right]$$

Where $\sigma_n = n_{out}(\mu^o_{out,g} - \mu^o_{bulk,g}) + n_s(\mu^o_{out,s} - \mu^o_{1,s})$ is essentially the "surface energy" of a gold particle containing *n* atoms. In the limit of large excess of surfactant (i.e., $X_s >> X_g$), the above relations can be further simplified by considering that $X_{1,s} \to X_s$, reducing the problem to one equation and one constraint, with which to determine α.

$$X_n = n \exp\left[(-\sigma_n + \alpha n) / k_B T + n_s \ln(X_s)\right]$$

$$\sum_{n=1} X_n = X_g$$

Importantly, this limiting case gives the minimum particle size for a given capping agent and is valid for experiments reported in the literature (e.g., $X_s = 0.03 >> X_g = 0.001$) (5).

Having outlined the approach, we must now estimate how both n_s and σ_n depend on the particle size *n*. First, the number of gold atoms *n* in a particle is related to the particle radius, *R* (where *R* is measured from the center of the particle to the end of the surfactant chain), by the following equation.

$$n = 4\pi(R - \delta)^3 / 3v_g$$

Where $\delta \approx 16$ Å is the length of the surfactant chain, and $v_g = 17$ Å^3 is the volume of each gold atom (4). Similarly, the number of surfactant molecules bound to the particle surface (assuming ideal monolayer coverage) is given as

$$n_s = 4\pi(R - \delta)^2 / A_s \sim n^{2/3}$$

where $A_s = 21.4$ Å is the area occupied by a single surfactant molecule.

Examining the expression for σ_n, the first term is associated with the surface energy of a bare gold particle (i.e., the energy difference between an atom at the surface and one in the bulk). This term should be of the form $An^{2/3} + Bn^{1/3}$ since it is proportional to the surface area (scales as $n^{2/3}$) via a curvature-dependent surface energy (of the form $C + D/(R-\delta)$ or $C + D'/n^{-1/3}$). The binding energies, E_n, of small gold clusters have been calculated theoretically (6) and are related to the desired surface energies by

$$\varepsilon n - E_n = An^{2/3} + Bn^{1/3}$$

Where, ε is the binding energy per atom in bulk gold. Therefore, A and B can be estimated by fitting the following relation to the reported data (cf. Fig. 8).

$$E_n / n = \varepsilon - An^{-1/3} - Bn^{-2/3}$$

From this analysis, we estimate A and B to be 1.8 and 2.8, respectively.

The second term of σ_n is associated with the lowering of the gold/solvent energy by the adsorption of surfactant on the gold surface. This term can be approximated as

$$n_s(\mu^o_{out,s} - \mu^o_{1,s}) = n_s\left[-E_{sg} + J/(R-\delta)^2\right]$$

Where E_{sg} is the free energy of the surfactant-gold bond (here, $E_{sg} > 1$), and J is related to the bending constant of the monolayer. The curvature-dependent term accounts for the reduction of dispersive (van der Waals) interactions in small particles and vanishes in the case of a flat surface. We chose $J = 43\text{Å}^2\ k_BT$, which corresponds to typical bending constants of amphiphilic monolayers and is exactly the value used previously to describe digestive ripening experiments (4).

Applying the methodology described above, we calculated particle size distributions for various binding energies E_{sg}. The Lagrangian multiplier, α, was determined numerically using a globally convergent implementation of Newton's method (7). Comparing the calculated relationship between the average particle size and the binding energy with the aforementioned experimental results (5), we estimate that the difference in binding energies is ~0.12 eV. From this energy difference, we estimate the ratio of adsorption equilibrium constants to be ~100, favoring the adsorption of the thiol over that of DDA.

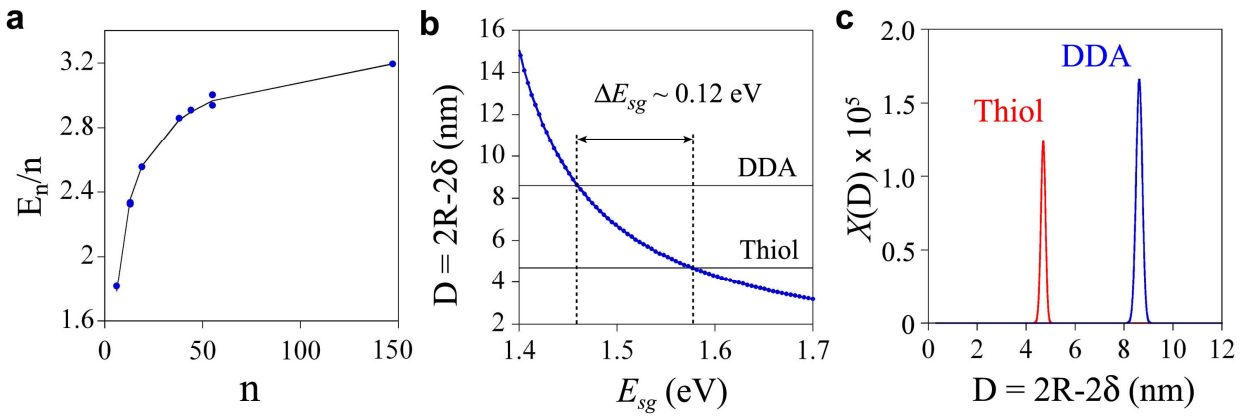

Figure 8. (a) Binding energy per atom as a function of gold cluster size, n. Data was obtained from Reference (6) by averaging results from the local density approximation (LDA) and the generalized gradient approximation (GGA). The fit corresponds to $E_n / n = \varepsilon - An^{-1/3} - Bn^{-2/3}$ with ε = 3.6 eV, A = 1.8 eV, and B = 2.8 eV. Note that while ε varies slightly from experimental measurements on bulk gold (ε_{exp} = 3.8 eV), it describes the asymptotic behavior ($n \to \infty$) of the model calculations. **(b)** Calculated particle diameter as a function of the surfactant-gold binding energy, E_{sg}. **(c)** Particle size distributions for thiol (E_{sg} ~ 1.58 eV) and DDA (E_{sg} ~ 1.46 eV) capping agents. The binding energy of the thiol agrees with theoretical estimates of the thiol-gold bond energy (~1 eV) (8) combined with the dispersional interactions between alkyl chains (~1 eV for $SC_{16}H_{33}$) (8).

Section 4. Competitive thiol adsorption.

4.1 In all experiments, *trans*-azobenzene dithiol (ADT) was mixed with gold nanoparticles (AuNP), dodecylamine (DDA) capping agent, and didodecyldimethylammonium bromide (DDAB) surfactant. After equilibration, the AuNPs were covered by a mixture of ADT and DDA (the adsorption of DDAB was negligible in comparison) whose composition depended on the relative amounts of DDA, ADT, and AuNP in solution. Because direct instrumental techniques were not feasible to determine the amounts of NP-bound ADTs. (e.g., relaxation times were too long for NMR, NPs were too small for Raman), we used thermodynamic reasoning supported by experiments described in Section 3 to determine concentrations of surface bund ADT ligands. Specifically, we estimated the fractional coverage of ADT by solving the equilibrium adsorption problem accounting for the *finite* number of ADT molecules and gold adsorption sites in solution. The equilibrium constants for the adsorption of ADT and DDA onto gold – K_T and K_D, respectively – are related to the equilibrium concentrations as follows.

$$K_D = \frac{[DS]}{[S][D]} \text{ and } K_T = \frac{[TS]}{[S][T]}$$

Where $[DS]$ and $[TS]$ represent, respectively, the concentrations of DDA and ADT adsorbed onto a gold site S, and $[D]$ and $[T]$ represent the concentrations of DDA and ADT in solution. Furthermore, the total number of gold sites and ADT molecules must be constant.

$$[S]_{total} = [S] + [DS] + [TS] \text{ and } [T]_{total} = [TS] + [T]$$

Due the excess of DDA in solution ($[D] >> [S]_{total}$), its concentration in solution remains unchanged to good approximation.

For the experiments discussed in the text, $[D]$ = 35 mM, [Au atoms] = 1.95 mM, and $[T]$ varied from zero to 2.4 mM. From the AuNP diameter (5.6 nm), we estimate that each particle contained ~5400 gold atoms and ~460 binding sites (assuming a binding area of 21.4 $Å^2$) (4). Therefore, the concentration of binding sites can be estimated as $[S]_{total}$ = 0.17 mM. Equilibrium adsorption constants for alkyl thiols on gold surfaces have been measured experimentally to be $K_T \sim 10^4$ M^{-1} (9). While there exist no experimental data for the adsorption of alkyl amines onto gold surfaces, we estimate (cf. Section 5 on digestive ripening) that $K_D \sim 10^2$ M^{-1} – i.e., about two orders of magnitude less than that of thiols. From these estimates, one can calculate the fractional surface coverage of ADT on the surface of the AuNPs.

$$\theta = \frac{\frac{1}{2}\left(K_D[D] - \sqrt{\begin{pmatrix} K_T{}^2[T]_{total}^2 - 2K_T{}^2[T]_{total}[S]_{total} + 2K_TK_D[T]_{total}[D] + 2K_T[T]_{total} + \ldots \\ K_T{}^2[S]_{total}^2 + 2K_TK_D[S]_{total}[D] + 2K_T[S]_{total} + K_D{}^2[D]^2 + 2K_D[D] + 1 \end{pmatrix}} + K_T[S]_{total} + K_T[T]_{Total} + 1 \right)}{K_T[S]_{total}}$$

Where θ is the fractional coverage of ADT (i.e., $[TS]$ / $[S]_{total}$). The plots below give the fractional coverage, θ (Fig. 9, left) and the numbers of ADT adsorbed onto one AuNP (Fig. 9, right). The upper and lower dashed lines in Fig. 9 indicate the ADT coverages corresponding to the lower and upper limits of LISA, respectively (cf. phase diagram in Fig 1a, main text). Note that while for $[T]$ = 1.2 mM (fraction coverage ~ 0.7) aggregates were formed, they did not form when the concentration was increased to 2.4 mM (fractional coverage ~ 0.85) – presumably due to the inability of *trans*-ADT to isomerize on the AuNPs' surface covered densely with ADT. Furthermore, the minimum concentration necessary for forming aggregates was ~ 0.02 mM, at which there were ~18 ADT molecules adsorbed onto each AuNP.

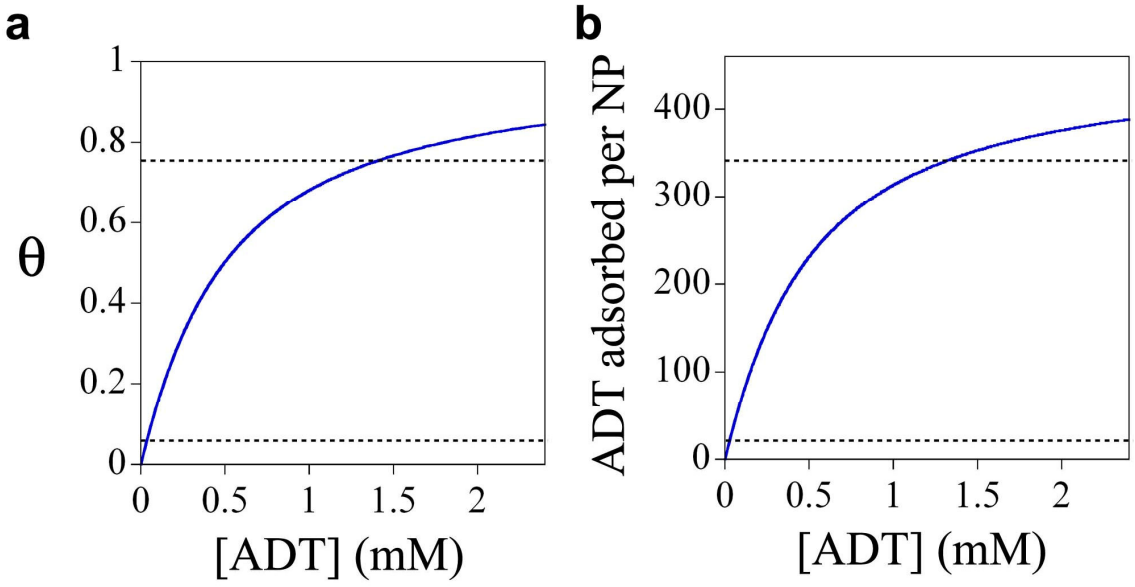

Figure 9. (a) Fractional surface coverage of ADT as a function of ADT solution concentration, calculated for [DDA] = 35 mM, [Au atoms] = 1.95 mM, $K_T \sim 10^4$ M^{-1}, $K_D \sim 10^2$ M^{-1}. **(b)** Number of ADT adsorbed per NP as a function of ADT solution concentration, calculated as described in Section 6 of the Supporting Information.

4.2 The above description of the competitive adsorption equilibrium is also helpful in explaining experimental observations regarding the LISA of NPs of various sizes. For example, in addition to experiments performed on 5.6 nm particles described in the main text, we conducted similar experiments using 8.0 nm particles using the same concentrations of Au atoms and DDA ligands. While the qualitative behavior of the larger particles was the same as that reported in the main text for smaller NPs, there were some *quantitative* differences. For instance, we found that for pure toluene solutions (i.e., no methanol) the 5.6 nm particles required ~2.5 times more ADT ligands in solution to aggregate (into *SS* phase under these conditions) than the 8.0 nm particles.

In these experiments, the concentrations of DDA and Au atoms were held constant ([DDA] = 35 mM and [Au atoms] = 1.95 mM), and the ADT concentrations were varied to find the critical concentrations necessary for aggregation (here, of supraspheres). For NPs of radii R_1 = 2.8 nm and R_2 = 4.0 nm, the critical ADT concentrations were found experimentally to be $[\mathrm{ADT}]_1^{crit}$ = 20 μM and $[\mathrm{ADT}]_2^{crit}$ = 8 μM, respectively. Recall from the above discussion, that the number of adsorbed ligands per NP, N_{azo}, depends on both the ADT concentration and on the concentration of adsorption sites, which itself depends on R as $C_{Sites} = C_{Au}(3v_g / A_S R)$, where C_{Au} is the gold atom concentration (here, held constant), v_g is the volume of each gold atom, and A_S is the area of a binding site. Thus from these data, the competitive adsorption model predicts $N_{\mathrm{azo}}([\mathrm{ADT}]_1^{crit}, R_1) \sim 14$ and $N_{\mathrm{azo}}([\mathrm{ADT}]_2^{crit}, R_2) \sim 13$ ADTs per NP. Therefore, it appears that ~13-14 ADT ligands are absolutely necessary for aggregation of particles regardless of their size – interestingly, this number is close to the coordination number of ~12 for dense hard sphere liquids or *hcp* crystals.

Section 5. Detailed discussion of the nucleation theory and the dependence of NP-aggregate sizes on ADT concentration.

We observed that irrespective of solvent polarity, the overall dimensions of either crystals or supraspheres decreased with increasing concentration of ADT ligands per NP (Fig. 3a). This effect is due to a nucleation-and-growth mechanism (10), in which the free NPs initially nucleate into small, thermodynamically unstable (unless larger than a critical size) clusters that subsequently grow by the addition of single NPs until all NPs available are used. According to this scenario, the average number of NPs per aggregate, $< N >$, can be estimated from the ratio of the initial concentration of NPs in solution, C_{NP}, and the equilibrium concentration of critical nuclei, C_{Nuc} – i.e., $< N > \sim C_{NP} / C_{Nuc}$. Assuming that the number of nucleation "sites" is proportional to the number of ADT molecules, C_{Nuc} is estimated from classical nucleation theory (11) as $C_{Nuc} \sim C_{ADT} \exp[-A\sigma^3 / \Delta\mu^2 kT]$, where A is a positive constant, σ is the specific surface energy between the aggregate phase and the free NP phase, and $\Delta\mu$ is the gain in free energy associated with the transfer of one NP from the free NP phase to the aggregate phase. While both σ and $\Delta\mu$ potentially depend on the surface coverage of ADT ligands, this dependence is only significant near $\Delta\mu \sim 0$, where the energetic gain of dipole-dipole interactions and ligand crosslinking is balanced by the entropic loss associated with aggregation (this corresponds to $C_{ADT} \sim C^*_{ADT}$ as described in the main text). For ADT concentrations below this limit ($\Delta\mu < 0$), there is no driving force for aggregation, and the NPs remain stable in solution. Above and near this limit, the concentration of nuclei increases rapidly with increasing $\Delta\mu$, and the average aggregate size *decreases* rapidly with increasing number of dithiol ligands per NP. For even larger ADT concentrations, however, the dependence of the exponential term on C_{ADT} is negligible, and the aggregate size is well approximated by $< N > \sim C_{NP} / C_{ADT}$ or, equivalently, $D \sim (C_{NP} / C_{ADT})^{1/3}$ as given in the main text.

Section 6. Transition between crystals and supraspheres.

6.1. To rationalize the transition between crystalline (*C*) and suprasphere (*SS*) phases on the basis of their free energies, we first note that these free energies comprise entropic and energetic terms. Specifically, the difference in the Gibbs free energy between the *C* and *SS* phases is given by $\Delta G = G_C - G_{SS} = (H_C - H_{SS}) - T(S_C - S_{SS})$, where *H* and *S* denote the enthalpy and entropy per NP, respectively, of either the crystalline (*C*) or the disordered suprasphere (*SS*) phases.

As verified by crystallography, the *C* phase is characterized by an *hcp* structure and a packing fraction ~0.74, for which the entropy per particle (for hard spheres) has been estimated previously by Hoover and Ree (12) to be $S_C \sim -6k$ (relative to an ideal gas at the same density and temperature). The *SS* phase is treated as a dense hard sphere fluid, characterized by a "loose" *hcp* ordering and a packing fraction of ~0.67 (this packing fraction represents an upper bound corresponding to a hard sphere fluid in equilibrium with an *hcp* solid), for which the entropy per particle is $S_C \sim -5k$ (12). Thus the entropic contribution to the free energy difference, ΔG, is estimated to be $T(S_C - S_{SS}) \approx -kT$.

Assuming the difference in molar volumes of the *C* and *SS* phases is negligibly small, the difference in per-particle enthalpies, ΔH, is identical to that of the internal (potential) energies, ΔE, of the aggregates. This quantity is estimated as the sum of bulk and surface terms, $\Delta E = E_C - E_{SS} \approx 0.5\Delta n E_{ad} + (A_C - A_{SS})_v \sigma_{agg}$ where Δn is the difference in the average number of nearest neighbors between the *C* and *SS* phases, E_{ad} is the adhesion energy of an NP pair (here, it is assumed that methanol molecules are present *in* the aggregates), A_C and A_{SS} are the surface areas of the same-volume *C* and *SS* aggregates, respectively, and σ_{agg} is their surface energy. The first term in this equation accounts for the potential energy of NP-NP interactions in each phase and is approximated as the sum of nearest-neighbor adhesion energies (more favorable for closely-packed *hcp* crystals than for randomly-packed supraspheres). The surface energy term is estimated as in Israelachvili (2) for planar closed packed surfaces, $\sigma_{agg} \approx -0.43 E_{ad} / R^2$, where *R* is the radius of the NPs, and it is assumed that the surface energies of the supraspheres and of the various crystal faces are identical. Comparing supraspheres with the same-volume, compact (minimal surface-to-volume ratio) crystals of experimentally observed morphologies (e.g., hexagonal plates in Fig. 2 A), the difference in

areas is roughly $A_C - A_{SS} \approx 0.18(4\pi R^2)$. With these simplifications, $\Delta E \approx (0.5\Delta n - 1)E_{ad}$, where $\Delta n > 0$ since the NPs are more loosely packed in the SS than in the C phase.

With these assumptions, $\Delta G = (0.5\Delta n - 1)E_{\mathrm{ad}} + kT$, such that the crystalline phase is favored for $\Delta G < 0$ (i.e., E_{ad} is sufficiently negative, $E_{\mathrm{ad}} < -kT/(0.5\Delta n - 1)$), and the suprasphere phase is favored for $\Delta G > 0$ (i.e., $E_{\mathrm{ad}} > -kT/(0.5\Delta n - 1)$). Furthermore, the relation $\Delta G = 0$ provides a rough prediction of the phase boundary, whose shape is in qualitative agreement with the experimentally observed boundary for reasonable estimates of $\Delta n \sim 2$ [specifically, $0 < \Delta n < 6$, where the lower and upper limits correspond to near-*hcp* packing (12) and random, "jammed" packing (13), respectively].

6.2. We note briefly that phase behavior similar to that observed in our system has been reported for colloid-polymer systems (14). In these systems, colloidal particles interact through purely attractive depletion forces, whose magnitude increases with increasing polymer concentration. Increasing the attractive interactions in such systems (analogous to increasing methanol content or ADT surface concentration in the present system) has been shown to induce phase transitions (see (13) and references therein) from the gas phase to condense phases – both liquid and crystalline – similar to the liquid-like *SS* phase and crystalline *C* phases observed in the present work. Further increase in the polymer concentration, however, has been shown to lead to kinetically-controlled aggregation processes, resulting in a variety of disordered aggregates. Similarly, in the present system, increasing the methanol content and ADT surface concentrations beyond the crystalline regime results in amorphous aggregates, which quickly precipitate from solution.

Section 7. Supporting Information References:

1. Vanoppen P, Grim PCM, Rucker M, DeFeyter S, Moessner G, Valiyaveettil S, Mullen K, DeSchryver FC (1996) *J Phys Chem* 100**:**19636-19641.
2. Israelachvili JN (1992) *Intermolecular And Surface Forces* (Academic Press, San Diego).
3. Carrillo E, Talanquer V, Costas M (1996) *J. Phys. Chem.* 100**:**5888-5891.
4. Leff DV, Ohara PC, Heath JR, Gelbart WM (1995) *J Phys Chem* 99**:**7036-7041.
5. Prasad BLV, Stoeva SI, Sorensen CM, Klabunde KJ (2003) *Chem Mat* 15**:**935-942.
6. Haberlen OD, Chung SC, Stener M, Rosch N (1997) *J Chem Phys* 106**:**5189-5201.
7. Press WH, Teukolsky SA, Vetterling WT, Flannery BP (1996) *Numerical Recipes in C* (Cambridge University Press, Cambridge, MA).
8. Sellers H, Ulman A, Shnidman Y, Eilers JE (1993) *J Am Chem Soc* 115**:**9389-9401.
9. Karpovich DS, Blanchard GJ (1994) *Langmuir* 10**:**3315-3322.
10. Mutaftschiev B (2001) *The Atomistic Nature of Crystal Growth* (Springer New York).
11. Kashchiev D (2000) *Nucleation: Basic Theory with Applications* (Butterworth-Heinemann, New York).
12. Hoover WG, Ree FH (1968) *J Chem Phys* 49**:**3609-3617.
13. Donev A, Cisse I, Sachs D, Variano E, Stillinger FH, Connelly R, Torquato S, Chaikin PM (2004) *Science* 303**:**990-993.
14. Anderson VJ, Lekkerkerker HNW (2002) *Nature* 416**:**811-815.